Tephra-stratigraphy and Ash Componentry Studies of Proximal Volcanic Products at Mount Tangkuban Parahu, Indonesia: An Insight to Holocene Volcanic Activity

Syahreza S. Angkasa [1,2], Tsukasa Ohba[1], Takumi Imura[1], Iwan Setiawan[3], Mega F. Rosana[4]

[1] Faculty of International Resource Science, Akita University, Japan.
[2] Department of Geological Engineering, Universitas Pertamina, Indonesia
[3]Research Center of Geotechnology, Indonesian Institute of Sciences (LIPI), Indonesia.
[4]Faculty of Geological Engineering, Universitas Padjadjaran, Indonesia

Corresponding author: syahreza_sa@imvolcs.com
Manuscript received: January, 25, 2019; revised: February, 25, 2019;
approved: May, 20, 2019; available online: September, 02, 2019

Abstract - Tangkuban Parahu Volcano is one of the most active volcanoes in West Java, Indonesia, although most of the recent eruptions were relatively mild (*e.g.* 2013 eruption). However, there is still little information from the volcanic products in the proximal area. Here, a new documentation from the proximal volcanic succession is provided, including tephra-stratigraphy, componentry analysis, and petrography of volcanic products. Detailed mapping of the proximal area shows that the volcanic products are predominantly composed of alternating fine-clay and coarse ash, lapilli tuff, and pyroclastic breccia within ten tephra units. Componentry of ash particles revealed the presence of five components, associated with hydrothermally altered lithics, oxidized lithics, coherent crystalline lithics, magmatic juvenile, and free crystal in entire eruptive products. These indicate that the subvolcanic hydrothermal system has been developed since the Holocene and associated with a continual introduction of magmatic intrusion. Petrographic observation shows the presence of hydrothermal minerals of quartz or silica accompanied by alunite and kaolinite, representing acidic alteration within the crater-conduit. The existence of a silicified zone indicates that the subvolcanic hydrothermal system played an essential role as a cap-rock of pressurized gas and steam at depth (200-500 m), whereas magmatic injection caused the vapour plume expansion. The observation concluded that the proximal volcanic succession captured the evidence of coupled phreatic and phreatomagmatic activities during the latest development of Mount Tangkuban Parahu.

Keywords: Tangkuban Parahu, tephra-stratigraphy**,** Holocene, volcanic, proximal

INTRODUCTION

Phreatic or hydrothermal eruption is a common volcanic event associated with the rapid release of a confined pocket of pressurized flashing water and steam below the crater in many stratovolcanoes worldwide (*e.g.*, Wohletz and Heiken, 1992; Brownee and Lawless, 2001). In some cases, phreatic eruption is related to the heated hydrous-rich zone (*e.g.*, aquifer, subvolcanic hydrothermal system) by a magmatic intrusion, which leads to vapour expansion, and the boiling of pore fluid and hydrous minerals (Brownee and Lawless, 2001; Jamveit *et al*., 2004; Lowernstern

et al., 2018). The significance of phreatic eruption is that the explosion occurs unexpectedly, thus may cause a lethal proximal hazard due to the absence of precursory signals from geophysical and geochemical monitoring (Barberi *et al.*, 1992; Marini, 1996). The most recent dramatic example is the 2014 eruption of Mount Ontake, Japan, with a total of 63 people dead or missing (Sanno *et al.*, 2015; Oikawa *et al.*, 2016).

Phreatic deposits are mostly identified from a field observation, presented as white and yellow colour tephra succession with a range of grain size from ash to block fragment (Maeno *et al.*, 2016; Oikawa *et al.*, 2018). There are also an increasing number of studies using componentry analysis of volcanic products to classify phreatic explosion from phreatomagmatic eruption (*e.g.*, Pardo *et al.*, 2014; Suzuki *et al.*, 2013; Alvarado *et al.*, 2016). Additionally, phreatic and phreatomagmatic eruptive products contain hydrothermally altered lithic fragments, which have particular importance as they provide a direct evidence for the subvolcanic hydrothermal conditions within the crater-conduit (*e.g.*, Ohba and Kitade, 2005; Ohba *et al.*, 2007). Consequently, careful observation of ash particles may give a valuable constraint on the process and an important role of the subvolcanic hydrothermal system leading to a volcanic eruption (Ohba and Kitade., 2005; Ohba *et al.*, 2007; Minami *et al.*, 2016).

At Tangkuban Parahu Volcano, an exotic surface manifestation within the active craters has become an attraction for many locals and international tourists to visit and stay in the vicinity of the volcano. Therefore, even a small-scale eruption can cause inevitable casualties for the society and infrastructures. Nineteen explosions were reported from 1829 to 2004, and the last eruption occurred in 2013 (CVGHM, 2016). However, it was not clear whether those volcanic activities were purely phreatic or phreatomagmatic. Moreover, it is challenging to recognize the historical and prehistorical tephra succession due to scarce documentation of the volcanic products (*e.g.*, Silitonga, 1973; Kusumadinata, 1979; Soetoyo and Hadisantono, 1992; Sunardi and Kimura,

1998; Kartadinata *et al.*, 2002). Therefore, this study aims to document the detailed tephra stratigraphy and composition of the volcanic products at Mount Tangkuban Parahu, Indonesia. The main focus was on the tephra succession at the proximal area, which captured the eruption history and mechanism in the past. Specifically, this is to answer several research questions that can be tested from detailed fieldworks, ash componentry, and petrographic analyses, as follow: 1) What is the nature of proximal stratigraphy of the Tangkuban Parahu Volcano? 2) What was the role of the subvolcanic hydrothermal system in the past? 3) Does magmatic intrusion contribute to a volcanic eruption?

Terminology

Subvolcanic hydrothermal systems are active hydrothermal systems underneath the volcanic edifice of stratovolcano (Ohba and Kitade, 2005). Volcanic products are ejected materials from all types of volcanic eruptions (*i.e.*, plinian, phreatic, phreatomagmatic). They contain a wide range of type of lithics and pyroclasts (*i.e.*, scoria and pumice). Volcanic ash is the smallest fragment of the volcanic products (<2 mm in diameter).

Overview of the Tangkuban Parahu Volcano

The Tangkuban Parahu is a shield-like stratovolcano (Figure 1a) and part of the Sunda Volcanic Complex (SVC), which includes the extinct Sunda and Burangrang Volcanoes. The volcano develops at the rear volcanic chain of Sunda volcanic arc, as a result of continuous subduction of the Indo-Australia Plate underneath Eurasian Plate with a speed of 6 - 7 cm/yr (Figure 2a) (Tregoning *et al.*, 1994; Hall, 2002).

The volcanic activity of Mount Tangkuban Parahu (Figures 2b and 2c) has been divided into three main episodes: 1) Pre-Sunda caldera, 2) Sunda caldera, and 3) Tangkuban Parahu (Van Bemmelen, 1949; Kartadinata *et al.*, 2002; Nasution *et al.*, 2004) (Figure 2c). The onset of the Pre-Sunda Caldera episode is still poorly understood. It began either Gelasian (Bemmelen, 1949) or Calabrian of ca. 1.105 Ma (Sunardi and Kimura,
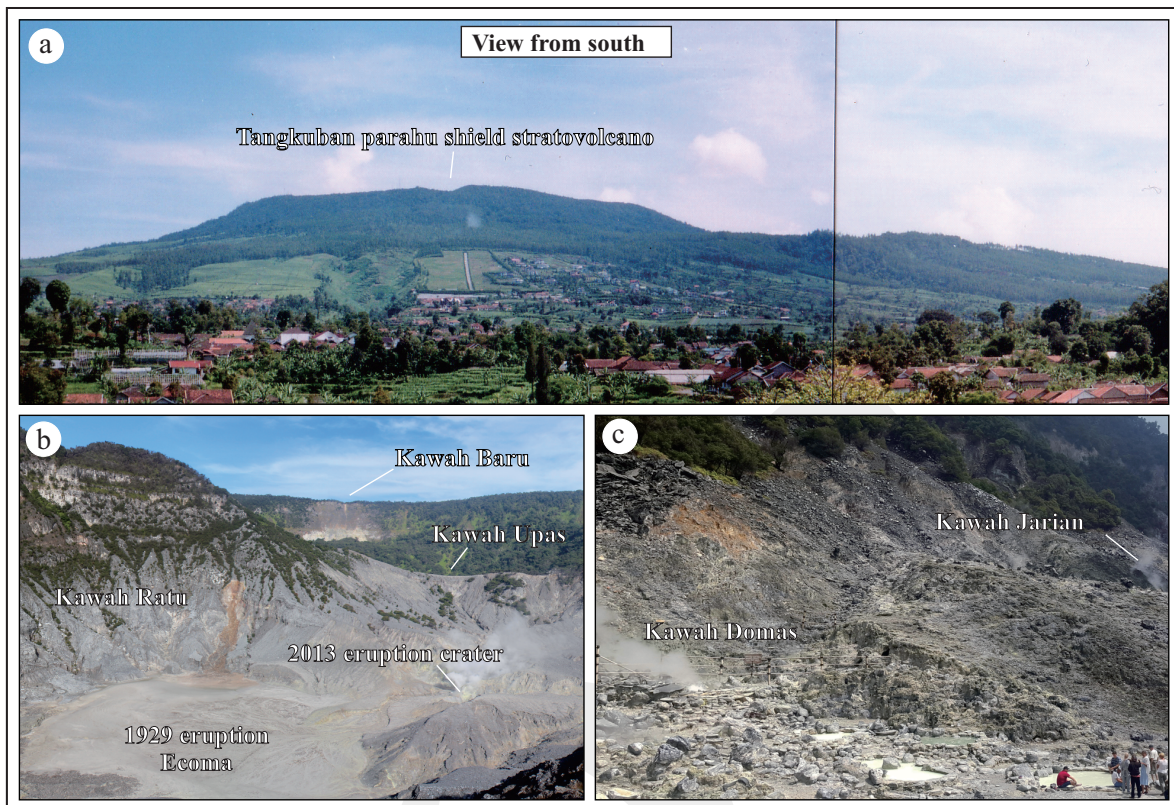
Figure 1. Photographs showing the Mount Tangkuban Parahu, Indonesia. a) A shield-like morphology of the stratovolcano (2084 m asl.) developed within the prominent arcuate caldera wall of Mount Sunda. (Photograph from N. Kartadinata); b) The volcano displays an extensive surface manifestation of the active hydrothermal system at several summit craters; c) as well as the parasitic craters (Domas, Jarian) at SE side of the summit. Moreover, most of the proximal deposits were derived from eruptions close to the Ratu crater, similar to the most recent 2013 eruption crater.

1998). The Pre-Sunda Caldera deposit comprising a series of pyroclastic rocks and lava flows (Batunyusun Lava Formation) unconformably overlies the Neogene sedimentary rocks (Subang Formation) (Figure 2c). The volcanic activity was terminated at 0.56 - 0.5 Ma (Sunardi and Kimura 1998), by the emplacement of caldera-forming Cisarua Ignimbrite (Kartadinata, 2005), which was then overlain by the Sunda volcanic group (Soetoyo and Hadisantono, 1992) from the Sunda caldera episode at 0.21 - 0.1 Ma (Kartadinata, 2005) (Figure 2c). The volcanic products of Sunda episode comprise lahar deposits, lava flows, and pyroclastic rocks, including a large volume of Manglayang ignimbrite deposit. Most of the eruptive products are widely distributed on the southern-northeastern of the prominent arcuate caldera wall.

The Tangkuban Parahu episode began at 0.09 Ma (Kartadinata *et al.*, 2002). It was mainly char-acterized by an explosive eruption associated with the magmatic, phreatomagmatic, and phreatic activities, as well as the effusive eruption of basaltic lava at 0.04 Ma (Sunardi and Kimura, 1998). The Old Tangkuban Parahu Formation comprises 30 tephra layers of pumice and scoria flow, that is associated with accretionary lapilli. These include nine major Plinian eruption periods (Kartadinata *et al.*, 2002), which were assumed to erupt from Upas and Badak craters, although it remains poorly understood. During the Holocene epoch, the volcanic activity is thought to be dominated by phreatic-explosions, which erupted from the separate craters (*e.g.*, Ecoma, Ratu, Siluman, Baru, Jarian) (Figure 1b and 1c). According to the brief description of Kartadinata *et al.* (2002), the Holocene volcanic products consist of interbedded sandy to clayey ash, altered ejecta, and base surge deposits.

Furthermore, recent surface expression of the volcano displays a massive hydrothermal activ-
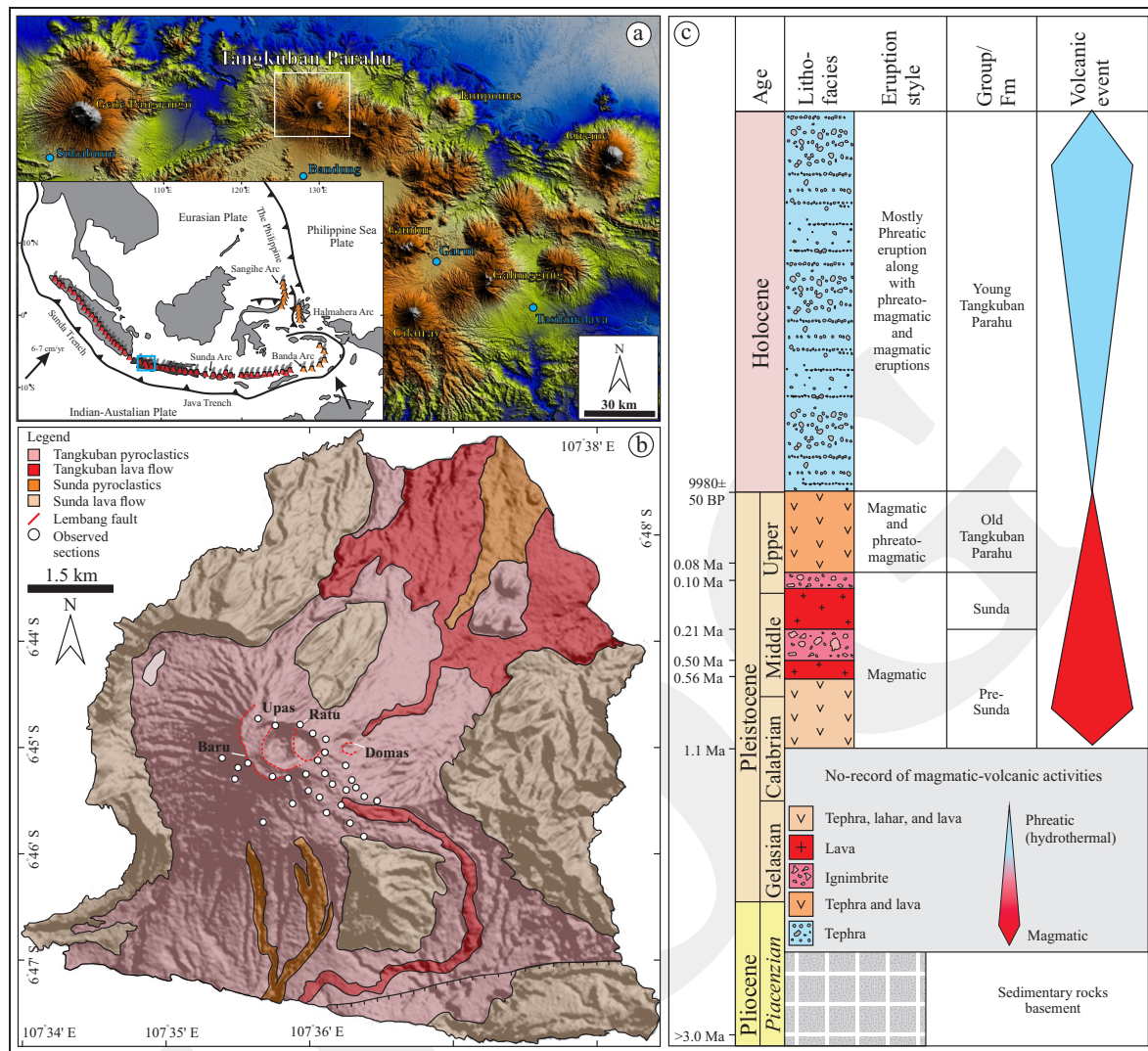
Figure 2. a) Map shows the location of the Mount Tangkuban Parahu, Indonesia, within the Sunda volcanic arc. b) Geological map of the Mount Tangkuban Parahu. The volcano is covered by a volcanic succession of explosive magmatic and phreatomagmatic eruptions from the Old Tangkuban Parahu Formation, whereas the younger volcanic products extend only ~1 km from the summit. c) Simplified stratigraphic overview of the studied area. The volcanic succession from the Pre-Sunda and Sunda Caldera episodes are based on a compilation from Van Bemmelen (1949), Soetoyo and Hadisantono (1992), and Sunardi and Kimura (1998). The Tangkuban Parahu episode was compiled in conjunction with a brief description of Kartadinata *et al*. (2002), Kartadinata (2005), and thickness is not to scale. For this study, the focus is on the Holocene volcanic activities younger than 10,000 B.P.

ity within the summit craters (*e.g.*, Ratu, Baru, Domas) (Figures 1b and 1c) by the persistence of solfataric and fumarole activity at a temperature of 90 - 100° C (Suryo, 1981 and 1985).

METHODS

Fieldwork

Field observation is focused on macroscopic volcanic facies (*e.g.*, McPhie *et al*., 1993), sort-ing, and grain size to diagnose the emplacement process of the volcanic products (Cas and Wright, 1987). The tephra succession is correlated based on the similarity of characteristics in each tephra layer, together with the presence of unconsolidated very fine- grained layer of paleosols (Miyabuchi, 2015).

Radiocarbon Dating

Charred-wood and charcoal were collected from two tephra layers at the crater rim (Figure 3,
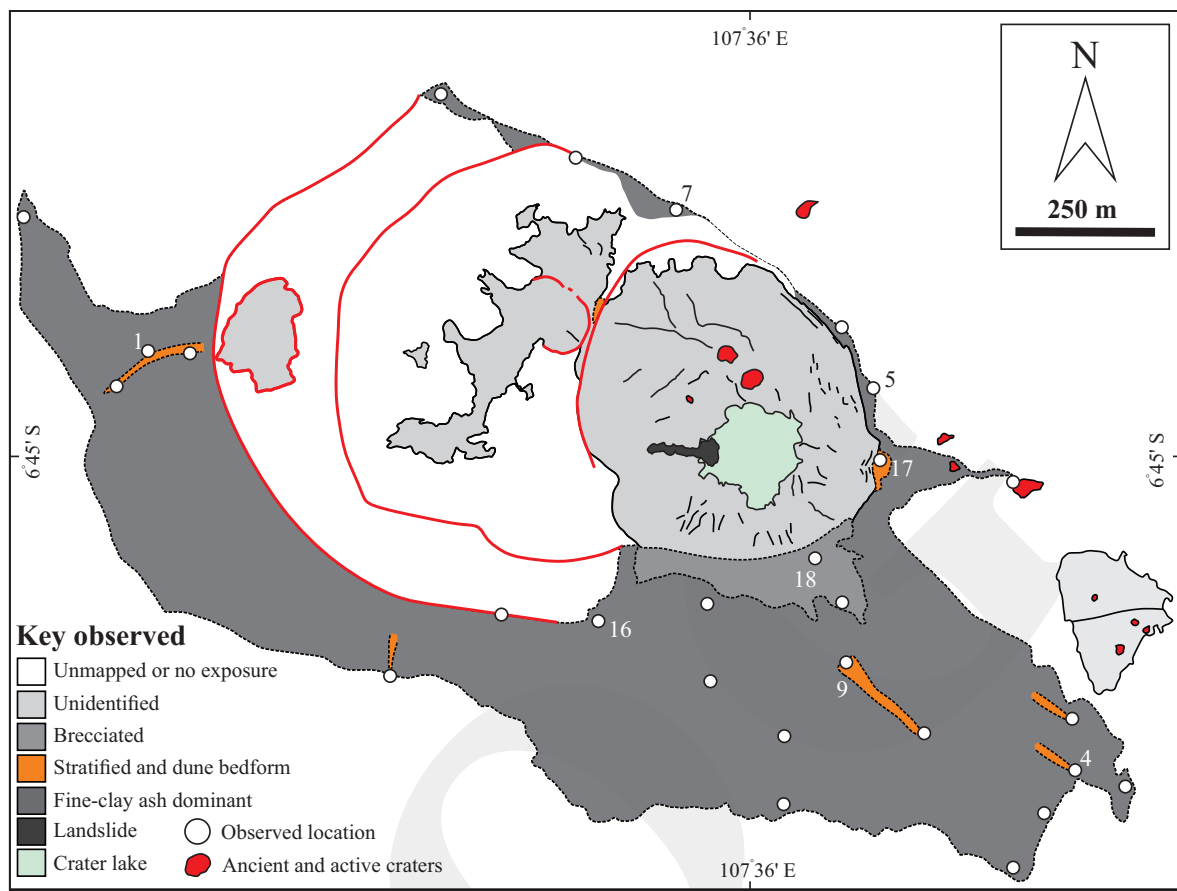
Figure 3. Geological map of the proximal area of Tangkuban Parahu Volcano displaying the observed locations and lithological distribution of volcanic products.

locations 5 and 17) for radiocarbon dating. These samples are used to provide the absolute age of those selected volcanic products. Both samples were handpicked in the field and placed into an aluminum foil container. Sample treatment using Acid-Alkali-Acid (AAA) and the measurement of ^{14}C concentration with Accelerator Mass Spectrometer (AMS) were undertaken at Beta Analytic Laboratory. Moreover, the ^{14}C ages were calibrated using IntCal13 (Reimer, 2013).

Sample Preparation and Analytical Techniques

A total of twenty-five volcanic products were sampled during the fieldwork with 50 - 100 g in-weight. Samples were entirely hand-sieved under wet condition into different mesh sizes ($-2 \leq \phi \leq 4.5$). Each fraction was bathed with distilled water and cleaned by an ultrasonic cleaner. These steps were repeated several times to clean the finer ash particles from coated clay and dust. Moreover,

cleaned ash fractions were dried with an oven at a temperature of 40° C for twelve hours.

Componentry analysis was carried out to classify the ash component and distinguish the phreatic explosion from the phreatomagmatic eruption based on components, whereas the petrography observation on some thin sections was performed to validate the component determination under a binocular microscope. For componentry analysis, the coarse ($1 \leq \phi \leq 2$) and fine ($3 \leq \phi \leq 4$) ash fractions were observed under a binocular microscope. The component of ash fraction was counted with a total of 1500 - 2000 grains to provide an adequate ash particle distribution. Volcanic ash was classified into several different types of components, according to their physical appearances (*e.g*., colour, alteration, volcanic texture; Ohba *et al*., 2007; Pardo *et al*., 2014; Suzuki *et al*., 2013; Alvarado *et al*., 2016).

Petrography of ash particles ($1 \leq \phi \leq 2$ and $3 \leq \phi \leq 4$) was studied using an optical and electron microscopes at the Faculty of International Resource Science, Akita University, with a scanning electron microscope (SEM, JSM-IT300, JEOL) equipped with an energy dispersive spectrometer (EDS, INCA X-act, Oxford Instrument). Microprobe analysis of minerals were carried out with an accelerating voltage of 15kV, a probe current of 2.2nA, a working distance of 10 mm, and a counting time of 30 - 80s, using cobalt for the standard.

RESULTS

Proximal Tephra-stratigraphy

In the proximal area, the volcanic succession consists of some mappable tephra units (Figure 3). Good outcrop exposures are located at the summit crater rim and towards the southern sector of the volcano within the radius of 0.5 - 1.5 km. For this study, a total of twenty-nine locations (Figure 3) were observed. These include re-observation of some locations that had been observed by Kartadinata *et al*. (2002) in the past. The tephra succession has a total thickness of ~4 m for the entire units. The lithologies are composed of fine-clay and coarse ashes, lapilli tuff, and pyroclastic breccia. They mostly show a massive structure, although some of the tephra units clearly display sedimentary structures (*i.e.*, cross stratification, dune bedform). The composite stratigraphy is shown in Figure 4.

Unit 1

Unit 1 is the lowest stratigraphic unit in this study, consisting of three tephra layers (Layers 1A, 1B, and 1C). Exposure of this unit is limited to Location 1 and 16 with a thickness of ~20 cm (Figure 5). Layer 1A is white to yellow fine-clay ash. It almost contains no lithic fragments. Layer 1B is grey coarse ash and 5 - 10 cm in thickness (Figure 6a). It displays a linear fabric of glassy fragments on a scale of <1 mm, which occur as characteristics of other tephra units. Layer 1C

is white to brown fine-clay ash (Figure 6a). It contains considerably high concentration (>20%) of lithic fragments. Moreover, lithics are wholly composed of angular to rounded altered fragments (<10 cm in diameter; Figure 6b).

Unit 2

Unit 2 consists of two tephra layers (Layer 2A and 2B) of fine-clay ash, which was observed at Locations 1, 16, and 18 (Figure 5). Both layers are different in colour, as well as the degree of grain cohesion. Layer 2A shows white to brown in colour with slightly loose fraction due to abundant embedded altered lithic fragments (<1 cm in diameter), whereas the Layer 2B displays white in colour, dense, and less abundant altered lithic fragments (<5 cm in diameter) (Figure 6c). The contact of these layers is obscure and appears as a normal grading structure (Location 1) (Figure 6c).

Unit 3

Unit 3 is yellow to red volcanic products, comprising three main tephra layers (3A, 3B, and 3C). Layer 3A is matrix-supported fine-clay ash. This layer contains block-sized altered and vesiculated lava fragments. The size of fragments decreases significantly towards the distal area (Location 9 to Location 4; Figure 5). Layer 3B is stratified dark-brown coarse ash, which occurs as a dune bedform along with local planar stratified laminae (Figure 6c). Each layer has a thickness of 5 - 20 cm with a total of ~1 m for entire succession. The deposit is predominantly distributed on the crater rim and significantly decreased in thickness towards the southern sector (10 - 20 cm in thickness). Layer 3C is yellow fine-clay ash, which rarely contains block-sized fragments (Figure 6c).

Unit 4

This unit is the thickest unit in the proximal area. It is composed of fine-clay ash, coarse, and lapilli tuff lithologies, which can separate into six tephra layers (Location 17, Figures 5, 6d, and 6f). Evidence of dormancy is absent from the unit, indicating a single emplacement period with a total thickness of ~1.5 m at the crater rim (Location 17).
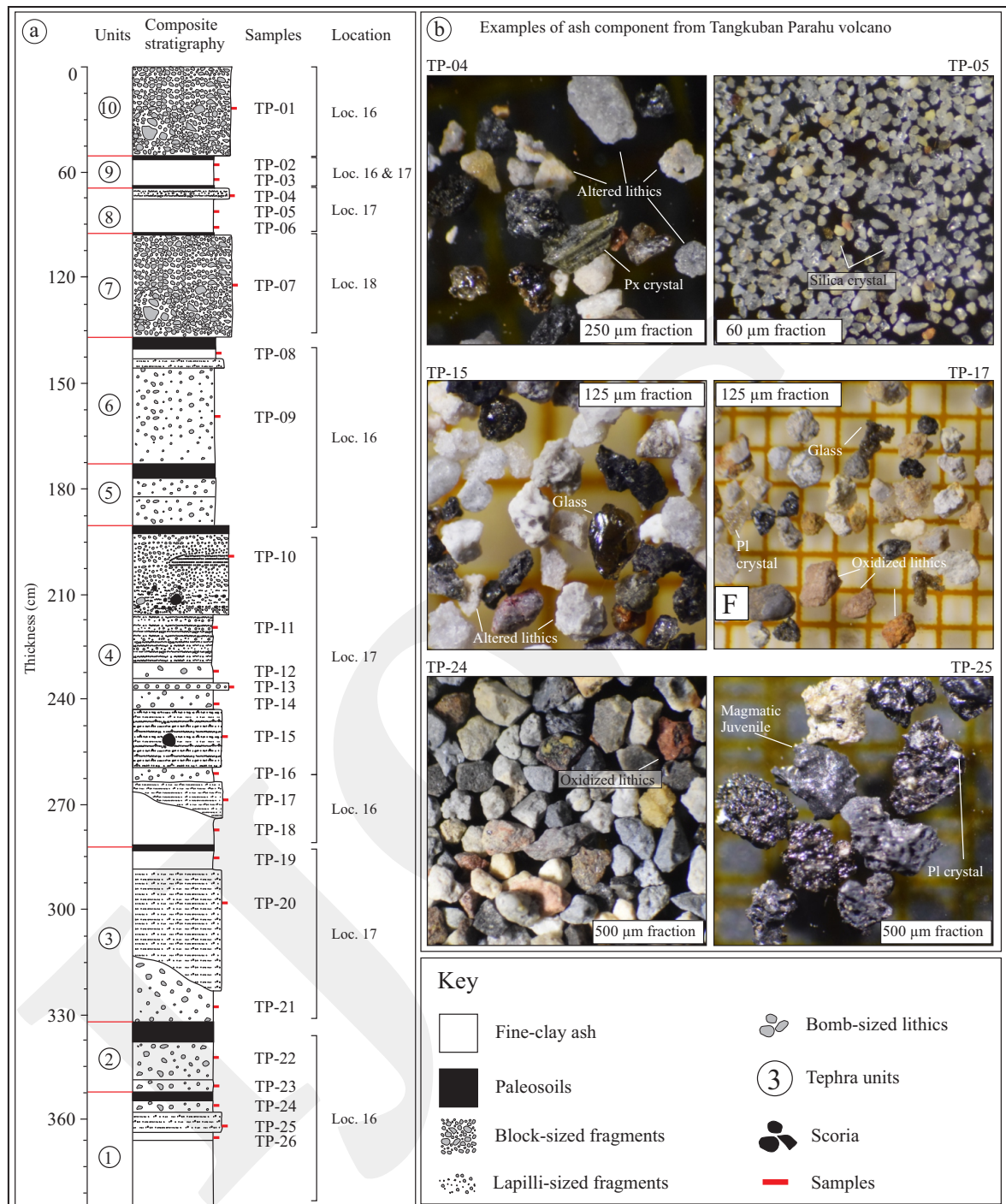
Figure 4. a) Composite tephra-stratigraphy of proximal deposits from three sections (locations 16, 17, and 18), including sampled horizons of the twenty-seven samples. B) Photographs showing the examples of volcanic ash from the volcanic products, comprising hydrothermally altered lithics, coherent crystalline lithics (*e.g.*, lava, hypabyssal rocks), oxidized lithics, free crystals (*e.g.*, quartz, pyroxene, quartz), and magmatic juvenile (*e.g.*, scoria, glass). All components are observed under the binocular microscope based on physical appearances (*e.g.*, Ohba *et al.*, 2007; Suzuki *et al.*, 2013).

Layer 4A is massive fine-clay ash, which rarely contains lapilli-sized altered fragments. Layer 4B is grey coarse ash and contains charcoal fragments. [14]C dating from a charcoal fragment yielded 982 - 904 cal BP (probability of 90.4%; see in Table 1.). Both Layers 4A and 4B are predominantly widespread throughout the southern sector within the radius of ~1 km. Layer 4C
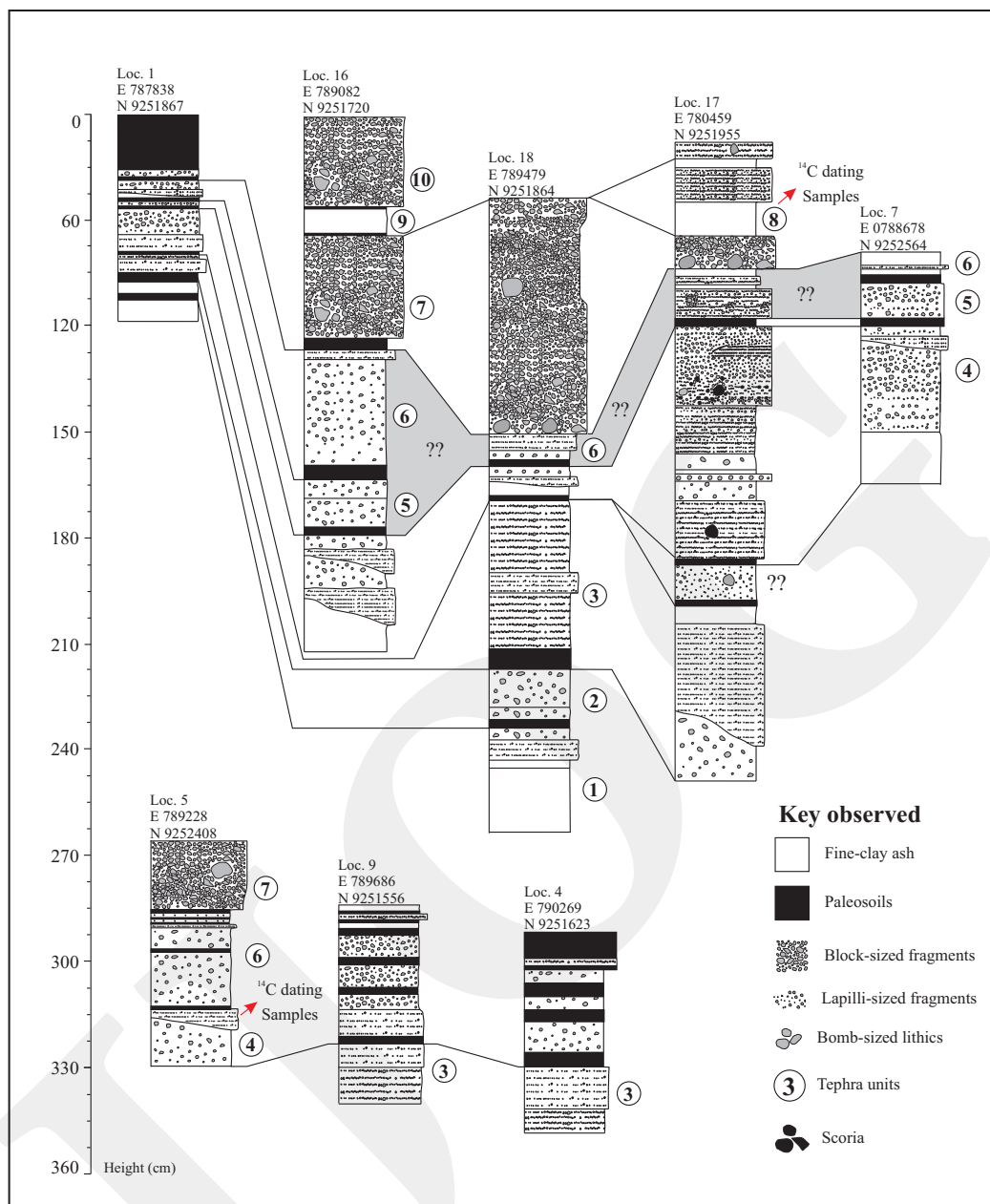
Figure 5. Detailed tephra-stratigraphic and correlation columnar sections of eight selected sections at the crater rim (Ratu and Upas) and southern flank of the summit crater. Each section exhibits a variety of volcanic units, separated by the presence of very thin weathered, loose, and organic-rich soil layers. The stratigraphy is divided into ten tephra units, although there are still several uncorrelated tephra-layers. The units are predominantly composed of fine-clay ash with lapilli-sized fragments, coarse ash, lapilli tuff, and pyroclastic breccia containing hydrothermally altered lithic clasts.

is massive white to yellow fine-clay ash. It is characterized by relatively poorly sorting and a slightly loose fraction due to abundant of altered lithics. Layer 4D is composed of an alternation of coarse ash (>5 cm in thickness) and fine-clay ash laminae (Figures 6 c, d, dan f). It hosts lithic blocks (>10 cm in diameter), which makes up 1% proportion for the entire layer. Layer 4E is

massive fine-clay ash, which is mostly encrusted by oxidation (Figures 6c and d). Layer 4F is a composite layer of stratified lapilli tuff, which is situated at the uppermost of Unit 4 (Figures 6c and d). Lapilli tuff layers display sedimentary structure, such as planar bedding along with local low-angle cross-stratification with a thickness ranging from 2 to 8 cm. It is interesting to note
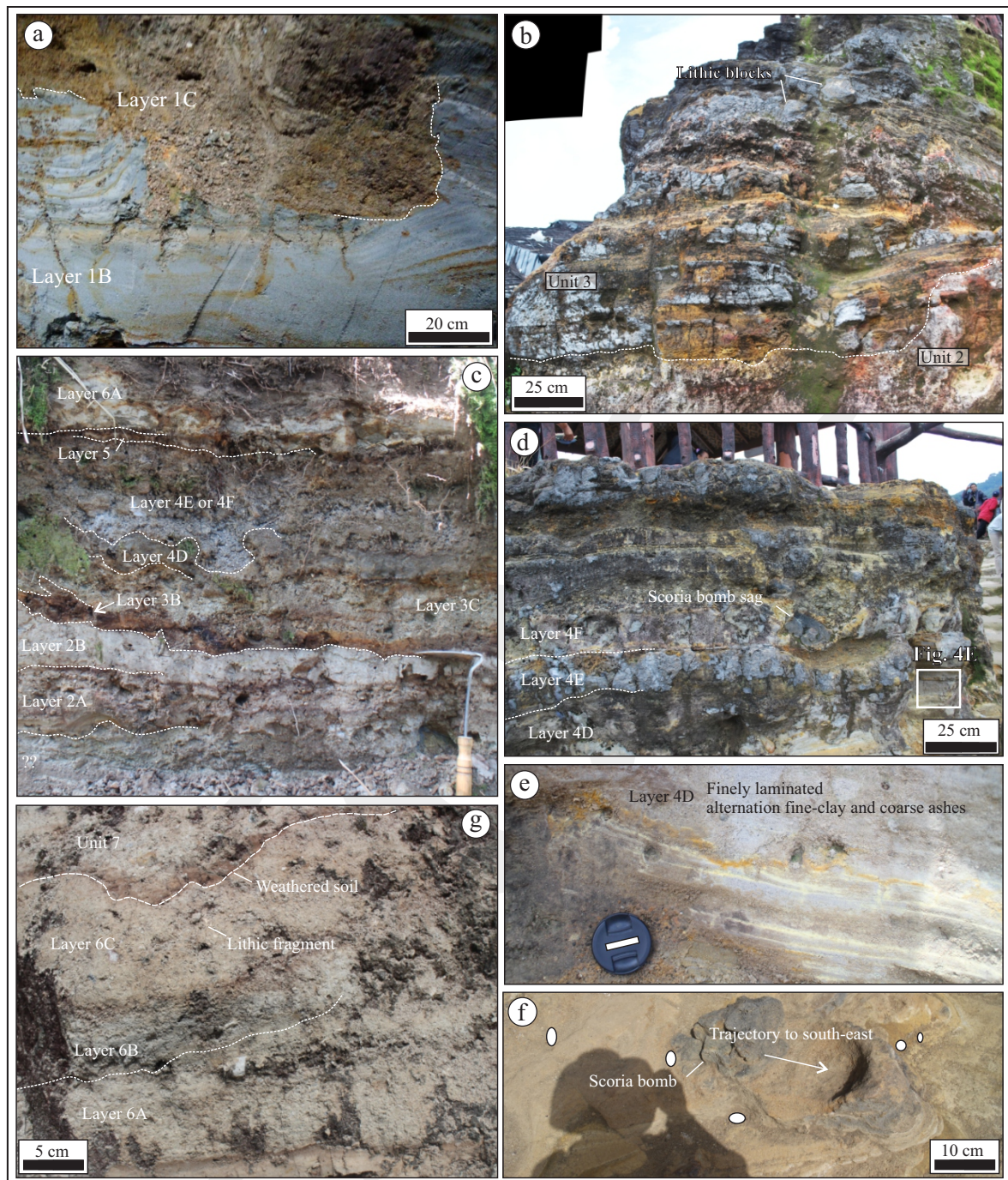
Figure 6. Photographs show examples of tephra outcrops in the proximal area. a) Irregular contact between coarse and fine-clay ash in Unit 1 (Layers 1A and 1B); b) as well as in Unit 2 and 3; c) Several tephra layers (Unit 2 to 6) occur on the western flank; d) Unit 4 is composed of an alternation of coarse ash and fine-clay ash (Layer 4); d) Fine-clay ash (Layer 4E), and stratified coarse ash (Layer 4F); e) Detailed photograph displays the fine-clay ash laminae along with coarse ash layers (Layer 4D), f) which includes sag structure of scoria in Unit 4; g) Coarse ash occurs as a lenticular structure in-between of fine-clay ash of Unit 6.

that Layers 4D and 4F contain scoria fragments (5 - 15 cm in diameter; Figure 6f), which frequently occur as a sag structure and represent the impact of ballistic during the eruption.

Unit 5

Unit 5 consists of two tephra layers (Layers 5A and 5B). Lithologically, it is matrix-supported fine-clay ash, which has similar characteristics to

Table 1. Summary of Radiocarbon Dating from Charred-wood and Charcoal in Volcanic Products

Sample ID	Samples	Tephra unit Layer	δ¹³C (‰)	Con. ¹⁴C age (yr BP)		Cal ¹⁴C age
TPCW-01	Charred	Unit 8	-26	111,44	0.42 pMC	1993 - 1998 cal AD (89.8%)
	wood	Layer 8A				1957 - 1958 cal AD (-5.6%)
TPCH-02	Charcoal	Unit 4	-23,3	1020	30	982 -904 cal BP (90.3%)
		Layer 4B				856-830 cal BP (4.1%)
						809 -803 cal BP (0.3%)
						1042-1038 cal BP (0.7%)

Unit 2. This unit is a typical volcanic product in the proximal area (Figure 6c). Both layers contain lapilli-sized fragments, although they are limited in Layer 5A than Layer 5B.

Unit 6

Unit 6 comprises three tephra layers (Layers 6A, 6B, and 6C; Figure 6g). Layer 6A is the fine-clay ash matrix with altered lithics (>1 cm in diameter; Figure 6c). It shows a white to yellow in colour and structurally massive. Layer 6B is finely-laminated coarse ash. The thickness varies from 5 to 30 cm. Layer 6C is white to yellow pyroclastic breccia.

Unit 7

Unit 7 is composed of massive pyroclastic breccia with a thickness of 2 - 3 m. It is abundant in clasts, up to 40 cm in diameter (Figures 6g, 7a, and 7b). Clasts are heterolithic, consisting of hydrothermally altered, vesiculated lava and rare scoria fragments within a clay-size matrix. The fragment concentration is higher (25 - 50%) at the base of the deposit, whereas the upper portion of the layer shows a lower fragment proportion (Figures 7a and 7b).

Unit 7

Unit 8 consists of four tephra layers (Layers 8A, 8B, 8C, and 8D). The lithology is an alternation of fine-clay ash and lapilli tuff (Figures 6c and 6d). All layers occur as a local mantle bedding at location 18 with 10 to 30 cm in thickness. Layer 8A is finely-laminated (<1 cm in thickness) fine clay ash with white to red colour (Figures 7c and d). Layer 8B is yellow to brown lapilli tuff,

which appears as a lenticular structure between Layers 8A and 8B. The charred-wood from Layer 8B yielded 111±0.42 pMC of modern carbon concentration, corresponding to calibrated age of post-1950 AD. Layer 8C comprises laminated fine clay ash, whereas the Layer 8D is lapilli tuff, containing subangular-shape altered lithics.

Unit 9

Unit 9 is a massive fine-clay ash (Figure 6e). This layer was observed only at location 16, which is situated in-between recognizable brownish paleosols. Unit 9 has a thickness of ~10 cm at the location 16.

Unit 10

Unit 10 is the youngest volcanic unit observed in this study. The lithology is massive white to grey pyroclastic breccia. Thickness ranges from 0.5 to 1 m (Figure 6e). It is predominantly distributed only at the summit, which is similar to Unit 7 and Unit 9. It is clast supported and wholly composed of hydrothermally altered lithic fragments with fine-clay ash as a matrix. The lithic fragments vary in size (10−20 cm in diameter), showing an angular to subrounded clasts shape.

Componentry Analysis

Componentry Classification

The schematic section with sampling horizons and photomicrographs of the ash particles is shown in Figure 4. Ash particles were divided into five type components; 1) hydrothermally altered lithics, 2) oxidized lithics, 3) coherent crystalline lithics, 4) magmatic juvenile, and 5) free crystal.
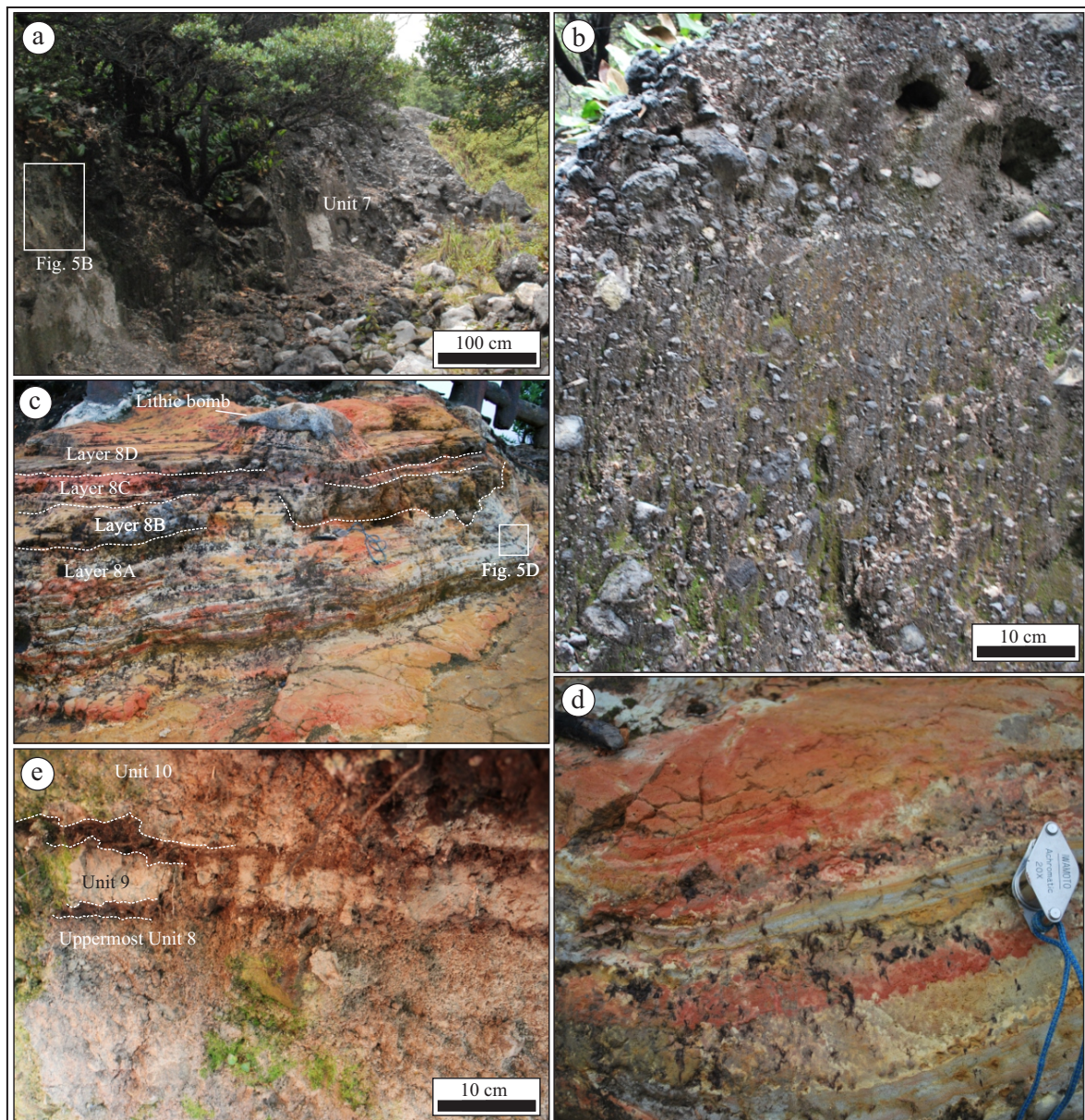
Figure 7. a) Photograph shows pyroclastic breccia of Unit 7. b) In Unit 7, clasts are abundant and heterolithic, which mainly concentrated at the top and base of Unit 7. c) Photograph shows the tephra layer of Unit 8, consisting of fine-clay ash and lapilli tuff. d) Detailed photograph shows a laminated structure of fine-clay ash in Layer 8A. e) Unit 8 to 10 are separated by very thin paleosols (1 - 3 cm in thickness).

Ash components are further described based on characteristics under microscopic observations (Figure 4b) as folows:

1. Hydrothermally altered lithics are present as white and yellow blocky fragments (TP-04 and TP-15). They mostly appear with vitreous and earthy luster, respectively.

2. Oxidized lithics are coated by brown to red stain (*i.e.*, coherent crystalline; magmatic glass; TP-17 and TP-24).

3. Coherent crystalline lithics display coherent rock textures (*i.e.*, phyric; aphyric) with earthy luster. They are possibly derived from several types of coherent rock (*i.e.*, extrusive and intrusive rocks).

4. Magmatic juvenile displays a vitreous luster with green and black colour, consisting of vesiculated and dense glass particles (TP-25). This component occurs as subangular-angular fragments and smooth surface of the

glass, together with substantially low vesicle textures (Figure 4, TP-15 and TP-25).

5. Free crystals are isolated minerals. For instance, the pyroxene grains appear as greenish orthorhombic crystal morphology (TP-04), whereas plagioclase grains occur as transparent and prismatic crystal (TP-17 and TP-25). Quartz is present as a subangular to subrounded, equant, and transparent crystals(TP-05).

Componentary Distribution

The distribution of ash component from the analyzed samples is shown in Table 2 and Figure 4. All samples contain the five components, although the proportion of components is somewhat scattered. Hydrothermally altered lithics are present within all samples and have a broad range of proportion (18%−93%) compared to the other components. The coherent crystalline lithics show a rather small proportion (<20%) in the samples. Oxidized and free crystal components generally display low proportions (<20%) from Unit 1 to Unit 7. However, their abundance shows anomalies in Unit 8 and Unit 10, which exceeds to higher percentages (>25%). Lastly, the presence of magmatic juvenile is fluctuative, ranging from 5% to 40 % in proportion. They prominently display a higher proportion in some samples from Unit 1 and Unit 4, whereas in other units their proportions are less (>5%).

Ash Petrography: Magmatic and Hydrothermal Minerals

Petrographic observation was carried out of the ash to specify the mineralogy, focusing on two mineral groups: 1) magmatic minerals and 2) hydrothermal minerals. More detailed mineralogy and petrography of the ash particles will be published in a separate article, exclusively for the hydrothermally altered fragments.

Magmatic minerals mostly occur in magmatic juvenile, coherent crystalline, and free crystal components. The magmatic juvenile comprises glassy groundmass and microlite crystals together with vesiculation textures, whereas coherent crystalline components show a volcanic rock

texture of porphyritic to pilotaxitic (Figures 8c and 8d). Magmatic minerals in magmatic juvenile and coherent crystalline lithics mostly share similar mineral assemblages. It comprises quartz, plagioclase, augite, ilmenite, rutile, and pigeonite (Figures 8a, 8c, and 8d). Even though, some of the analyzed coherent crystalline lithics have sanidine occurring in interstitial of quartz as the dominant mineralogical assemblages, they also contain xenocrystic subhedral-euhedral biotite crystals (>50 μm) together with euhedral plagioclase and quartz crystals (Figure 8d). Quartz crystals in the coherent crystalline components are an igneous origin (Figure 8b), characterized by euhedral and equant shape, containing single-phase inclusion of melt or glass (Figure 8f).

Hydrothermal minerals are composed of an association of silica (possibly quartz), alunite, and kaolinite, together with accessory minerals of TiO_2 and pyrite. Association of silica and alunite are abundant (Figure 8e). Some of the silica minerals were determined by using an optical microscope as a quartz crystal. Here, quartz crystals are the hydrothermal origin, which shows a mosaic-texture (Figure 8f), consisting of interlocked euhedral-equant shape quartz crystals (<10 μm in diameter). Alunite crystals occur as euhedral to subhedral, and equant to elongated lath (5 - 20 μm in length) crystals along with oscillatory zoning texture suggested from BSE image. Pristine kaolinite mostly occurs as very fine crystal (<1 μm) and commonly mixed with silica minerals. Accessory minerals are mostly anhedral (<5 μm in diameter) and disseminating on the surface of quartz-dominated ash particles.

DISCUSSION

Nature of Proximal Tephra-stratigraphy

The vast majority of volcanic successions at the proximal area of Tangkuban Parahu Volcano consists of an alternation of fine-clay and coarse ashes, lapilli tuff, and pyroclastic breccia. Massive fine-clay ash appears to be dominant in all volcanic products. In some units, the fine-clay ash is alternated with coarse ash. They predominantly show

Table 2. Summary of Componentry Analysis from Twenty-five Volcanic Products

Sample ID	Tephra unit	Lithologies	Hydrothermally altered		Coherent crystalline		Magmatic juvenile	Oxidised	Free crystal	Total counting
			White	Yellow	Phyric	Aphyric				
TP-01	Unit 10	Pyroclastic breccia	809	348	9	311	0	119	243	1839
TP-02	Unit 9	Fine-clay ash	150	179	6	44	0	174	1280	1833
TP-04	Unit 8	Lapilli tuff	1200	662	3	87	45	10	78	2085
TP-05		Fine-clay ash	347	202	8	42	0	267	889	1755
TP-06		Fine-clay ash	336	10	9	3	18	786	320	1482
TP-07	Unit 7	Pyroclastic breccia	757	1107	0	18	30	22	24	1958
TP-09	Unit 6	Fine-clay ash	708	674	12	288	60	100	40	1882
TP-10	Unit 4	Lapilli tuff	760	237	35	195	714	0	320	2261
TP-11		Lapilli tuff	358	402	10	347	650	79	130	1976
TP-12		Fine-clay ash	730	296	8	254	780	64	96	2228
TP-13		Lapilli tuff	1034	446	10	110	380	37	80	2097
TP-14		Fine-clay ash	760	237	35	195	714	0	320	2261
TP-15		Coarse ash	800	208	10	220	572	46	76	1932
TP-16		Fine-clay ash	659	311	14	60	714	98	320	2176
TP-17		Coarse ash	407	402	14	116	609	80	145	1773
TP-18		Fine-clay ash	810	768	15	104	44	212	38	1991
TP-19	Unit 3	Fine-clay ash	708	674	12	288	60	100	40	1882
TP-20		Coarse ash	934	664	12	95	170	10	80	1965
TP-21		Fine-clay ash	1020	760	2	28	20	198	98	2126
TP-22	Unit 2	Fine-clay ash	1200	662	3	87	45	10	78	2085
TP-23		Fine-clay ash	765	929	4	264	0	94	22	2078
TP-24	Unit 1	Fine-clay ash	869	817	17	185	0	58	54	2000
TP-25		Coarse ash	587	173	6	351	650	79	130	1976
TP-26		Fine-clay ash	530	689	2	105	567	81	172	2146
TP-27		Fine-clay ash	902	476	16	330	67	143	69	2003

the irregular contact together with finely-laminated structure, wherein some locations show as lenticular structures. Their emplacement is mostly associated with the lapilli to block-sized lithic fragments (*e.g.*, pyroclastic breccia; upper composite stratigraphy). Their concentration decreases toward to distal area (<1.5 km) (*i.e.*, Unit 2, Unit 3), which is very common for the volcanic products from the low-explosive intensity (*e.g.*, Maeno *et al.*, 2016; Oikawa, 2018). However, it is still challenging to understand their emplacement process (*e.g.*, fall-out, flow) due to the limited observed locations and mostly closed the sourced-vent (Ratu crater). Unit 3 and Unit 4 show very distinct sedimentary structures. Unit 3 display a prominent dune-bedform structure at the crater rim, whereas
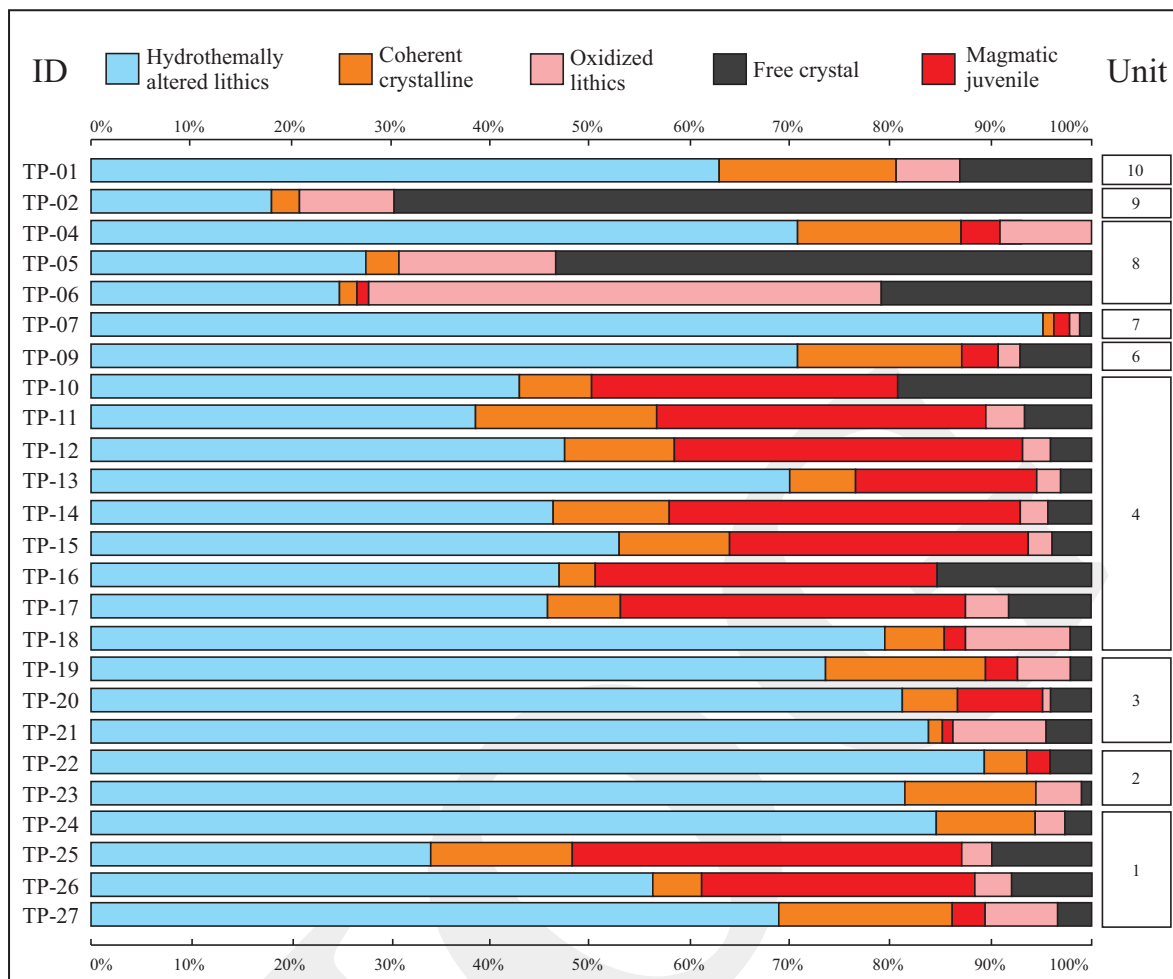
Figure 8. Diagram showing the results of componentry analysis with the total n=1400−2000 ash particles.

Unit 4 displays a planar and low-angle cross stratification of lapilli tuff. Both units indicate that they were emplaced as a pyroclastic base surge. In Unit 4, sagging structure by scoria fragments suggests that the volcanic product was deposited under wet condition (Cas and Wright, 1987).

Overall, the nature of proximal volcanic succession suggests that the past eruptions are predominantly composed of an intensive explosive eruption, which is associated with phreatic and phreatomagmatic events. These results are mostly consistent with the previous observation at Tangkuban Parahu Volcano (Kartadinata *et al*., 2002).

Role of the Hydrothermal System

Hydrothermally altered lithics are present in all volcanic products, which were suggested from componentry analysis. It indicated that

the hydrothermal system has been very active in the prehistorical time. From petrography, the hydrothermally altered fragments contain silica and alunite as a dominant hydrothermal mineral, indicating advanced argillic alteration is (Arribas, 1995; Hedenquist and Taran, 2013) extensively present at the crater conduit. This is similar to surface hydrothermal zonation at active craters (Syahidan *et al*., 2015). Silica (quartz), alunite, and kaolinite are precipitated from acidic vapor (*e.g.*, SO_2/H_2; $HCL/NaCl$) under a low-pressure condition, which encountered the country rock and produced extreme alteration effectively by hydrolysis reaction. The process reflects a range of formation temperature from 100 to 300° C (Arribas, 1995), which present near surface and surface of mature stratovolcano edifice (*e.g.*, Hedenquist and Taran, 2013).

Advanced argillic alteration is predominantly accompanied by an enormous amount of residual silica precipitation (White and Hedenquist, 1995).

One of the most notable observations on components (Figure 9) is that hydrothermally altered lithics are abundant in Unit 1 to 7, whereas they partly
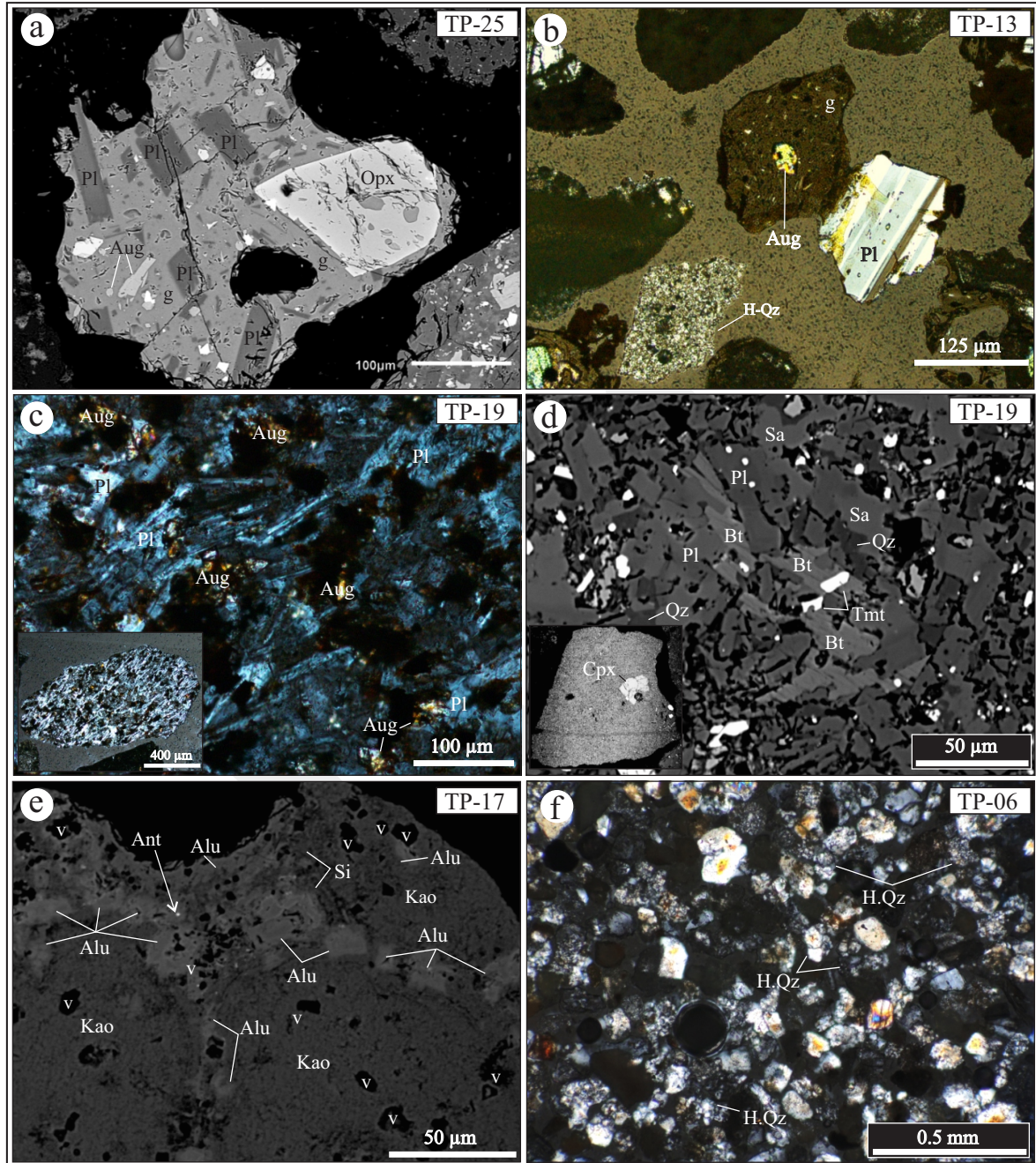

Figure 9. Photomicrographs and backscattered images showing the petrography of ash fractions. a) A BSE image showing the magmatic juvenile fragment with vesicular texture, consisting of orthopyroxene bearing glass inclusion, plagioclase, augite, and ilmenite within the andesitic glass. b) Magmatic juvenile fragments are predominantly present accompanying the mosaic-hydrothermal quartz. c) The pilotaxitic texture of coherent crystalline lithics consists of lath-shaped plagioclase, subhedral-euhedral augite, and ilmenite. d) A BSE image showing the porphyritic texture of coherent crystalline lithics, consisting of plagioclase, quartz, clinopyroxene, and xenocryst of biotite. e) Hydrothermally altered lithics predominantly comprising silica, alunite, kaolinite, and anatase. f) Coexistences magmatic-quartz with mosaic-hydrothermal quartz from the TP-08 sample, the free-crystal rich tephra layers. Abbreviation; *Aug:* augite, *Alu:* alunite, *Bt:* biotite, *Cpx:* clinopyroxene, *Kao*; kaolinite, *M-Qzt*: magmatic-quartz, *H-Qzt:* hydrothermal-quartz, *Pl:* plagioclase, *Si:* silica (unidentified polymorph).

replaced by abundant free crystals of hydrothermal quartz in Unit 8 and 10. This observation indicates extensive silicification at the crater conduit before the eruptions, which provides a capacity to cap or isolate the steam or gasses produced by the hydrothermal activity. If build-pressure of hydrothermal fluid overcomes the yield strength of the cap rock, failure of overburden rock leads to the sudden decompression, which results in an explosive phreatic eruption. Therefore, the volcanic products contain abundant fragments derived from the cap rock (*e.g.*, silicified rock).

Magmatic Contribution

The magmatic juvenile is observed from the componentry analysis. Cashman and Hobblit (2004) suggested that even a small proportion of magmatic juvenile can indicate the presence of a shallow intrusion. Therefore, the contribution of magmatic intrusion should also be considered for the volcanic eruptions of studied tephra stratigraphy. The magmatic juvenile is considerably present in many samples and shows a prominent proportion in Unit 1 and Unit 4. This indicates the periodic introduction of magmatic intrusion to the shallow volcanic edifices. The hydrothermally altered lithics also occur together with the magmatic juvenile, indicating fragmentation of altered country rocks during the volcanic eruption. Most of the magmatic juvenile fragments mostly are present as a dense fragment together with a smooth glass surface, suggesting magma-water interaction (Heiken and Wohletz,1985). Moreover, the presence of vesiculation texture on the magmatic juvenile indicates volatile release, which happens during the ascent of magmatic intrusion (*e.g*., Alvarado *et al*., 2016) and is also responsible for the overpressurized condition at the crater conduit due to vapour plume expansion below the crater (*e.g.*, Henley and Berger, 2011).

CONCLUSION

This study presented the field observations on the proximal tephra stratigraphy, componentry analysis, and petrography of volcanic product from Mount Tangkuban Parahu. The following are concluded based on the observation;

Volcanic products at proximal area consist of ten tephra units, comprising fine clay and coarse ash, lapilli tuff, and pyroclastic breccia. Their presence indicates the intense explosive eruption in the past, which is mostly distributed close to the summit craters.

The volcanic products are composed hydrothermally of altered lithics, oxidized lithics, coherent crystalline lithics, magmatic juvenile, and free crystal, indicating a complex process during the eruption process, involving fragmentation of country rock (hydrothermally altered zonation) and contribution of magmatic intrusions.

The hydrothermal fluid affects the system of crater conduit and precipitates silica or quartz, alunite, and kaolinite. Abundant silicified lithics and quartz crystals imply a significant role of silicified cap rock before sudden decompression of hydrothermal fluid.

The presence of magmatic juvenile in many tephra layers indicates the periodic introduction of magmatic intrusion into the shallow of volcanic edifices. The intrusion might have changed the condition of the hydrothermal system due to degassing from magma, resulting in vapour plume expansion.

Phreatic explosion appears to be a dominant eruption type for the entire volcanic products at the proximal area, although a few pulses of phreatomagmatic eruptions were also observed from field and componentry observation, which was recorded from Units 1 and 4 (c. 982−904 cal B.P.).

REFERENCES

Alvarado, G., Daniela, M., Pierfrancesco, D., Moor, J. M. D., and Geoffroy, A., 2016. Are the ashes from the latest eruptions (2010-2016) at Turrialba Volcano (Costa Rica) related to phreatic or phreatomagmatic events? *Journal of Volcanology and Geothermal Research*, 327, p.407-415. DOI: 10.1016/j.jvolgeores.2016.09.003.

Arribas Jr., A., 1995. Characteristics of high-sulfidation epithermal deposits, and their relation to magmatic fluid. *Mineralogical Association of Canada Short Course*, 23, p.419-454.

Barberi, F., Bertagnini, A., Landi, P., Principe, C., 1992. A review on phreatic eruptions and their precursors *Journal of Volcanology and Geothermal Research*, 52 (4), p.231-246. DOI: 10.1016/0377-0273(92)90046-G

Browne P.R.L. and Lawless, J.V., 2001. Characteristics of hydrothermal eruptions, with examples from New Zealand and elsewhere. *Earth Science Review*, 52, p.299-331. DOI: 10.1016/S0012-8252(00)00030-1.

Cas, R.A.F. and Wright, J.V., 1987. *Volcanic succession (modern and ancient)*. Allen and Unwin, London, 528pp.

Cashman, K.V. and Hoblitt, R.P., 2004. Magmatic precursors to the 18 May 1980 eruption of Mount St. Helens, USA. *Geology*, 32 (2), p.141-144. DOI: 10.1130/g20078.1.

Centre for Volcanology and Geological Hazard Mitigation, 2016. Database of volcanoes in Indonesia. *CVGHM Report*.

Hall, R., 2002. Cenozoic geological and plate tectonic evolution of SE Asia and the SW Pacific: Computer-based reconstructions, model and animation. *Journal of Asian Earth Sciences*, 20 (4), p.353-341. DOI: 10.1016?S1367-9120(01)00069-4

Hedenquist, J. and Taran, Y., 2013. Modeling the formation of advanced argillic lithocaps: volcanic vapor condensation above porphyry intrusions. *Economic Geology*, 108, p.1523-1540. DOI:10.2113/econgeo.108.7.1523.

Heiken, G. and Wohletz, K., 1985. *Volcanic ash*. University Presses of California, Chicago, Harvard and MIT, London, 285pp.

Henley, R.W. and Berger,B.R., 2011. Magmatic-vapor expansion and the formation of high-sulfidation gold deposits: Chemical controls on alteration and mineralization; *Ore Geology Reviews*, 39, p.63-74. DOI: 10.1016/j.oregeorev.2010.11.003.

Jamtveit, B., Svensen, H., Podladchikov, Y.Y., and Planke, S., 2004. Hydrothermal vent complexes associated with sill intrusions in sedimentary basins. In: Breitkreuz, C. and Petford, N. (eds) *Physical Geology of High-Level Magmatic Systems*. Geological Society of London, Special Publications. DOI: 10.1144/GSL.SP.2004.234.01.15.

Kartadinata, M.N., Okuno, M., Nakamura, T., and Kobayashi, T., 2002. Eruptive history of Tangkuban Parahu Volcano, West Java, Indonesia: A preliminary report; *Journal of Geography*, 111, p.404-409.

Kartadinata, M.N., 2005. *Tephrochronological study on eruptive history of Sunda-Tangkuban Parahu volcanic complex, West Java, Indonesia*. Doctoral Dissertation, Kagoshima University.

Koesoemadinata, K., 1979. Database of volcanoes in Indonesia. *Volcanological Survey Indonesia*, Bandung, 820pp.

Lowenstern, J.B., van Hinsberg, V., Berlo, K., Liesegang, M., Iacovino, K., Bindeman,

I., and Wright, H.M., 2018. Opal-A in glassy pumice, acid alteration, and the 1817 phreatomagmatic eruption at Kawah Ijen (Java), Indonesia. *Frontiers in Earth Science*, 6 (11), p.1-21. DOI:10.3389/feart.2018.00011)

Maeno, F., Nakada, S., Oikawa, T., Yoshimoto, M., Komori, J., Ishizuka, Y., Takeshita ,Y., Shimano, T., Kaneko, T., and Nagai, M., 2016. Reconstruction of a phreatic eruption on 27 September 2014 at Ontake Volcano, central Japan, based on proximal pyroclastic density current and fallout deposits. *Earth, Planets, and Space*, 68, article 82. DOI: 10.1186/s40623-016-0449-6.

Martini, M., 1996. Chemical characters of the gaseous phase in different stages of volcanism: precursors and volcanic activity. In: Scarpa, R. and Tilling, R. (eds), *Monitoring and mitigation of volcanic hazards*, Springer, Berlin Heidelberg, New York, p.199-219.

McPhie, J., Doyle, M., and Allen, R., 1993. *Volcanic textures: a guide to the interpretation of textures in volcanic rocks*. Hobart, Tasmania. Centre for Ore Deposit and Exploration Studies, University of Tasmania, 198pp.

Minami, Y., Imura, T., Hayashi, S. and Ohba, T. 2016. Mineralogical study on volcanic ash of the eruption on September 27, 2014 at Ontake volcano, central Japan: correlation with porphyry copper systems. *Earth, Planets, and Space*, 68, p.173-180. DOI: 10.1186/s40623-016-0440-2.

Miyabuchi, Y., 2015. Identification of paleosols around volcanoes dominating long-term small ash emissions: a case study from Aso Volcano, Japan; Special section determination of the construction of an outcrop database to reveal Eruptive History, *Bulletin of the Volcanological Society of Japan,* 60, p. 173-180. DOI: 10.18940/kazan.60.2_173 (written in Japanese with English abstract).

Nasution, A., Kartadinata, M.N., Kobayashi, T., Siregar, D., Sutaningsih, E., Hadisantono, R., and Kadarsatia, 2004. Geology, age dating, and geochemistry of the Tangkuban Parahu Geothermal Area, West Java, Indonesia. *Journal Geothermal Resource Society of Japan*.

Ohba, T., Taniguchi, H., Miyamoto T., Hayashi, S., and Hasenaka, T., 2007. Mud plumbing system of an isolated phreatic eruption at Akita Yakeyama volcano, northern Honshu, Japan. *Journal of Volcanology and Geothermal Research*, 161 (1), p.35-46. DOI: 10.1016/j.jvolgeores.2006.11.001.

Ohba, T. and Kitade, Y., 2005. Subvolcanic hydrothermal systems: Implications from hydrothermal minerals in hydrovolcanic ash. *Journal of Volcanology and Geothermal Research*, 145(3-4), p.249-262. DOI: 10.1016/j.jvolgeores.2005.02.002.

Oikawa, T., Ohba, T., Fujinawa, A., and Sasaki, H., 2018. Geological study of phreatic eruptions. *Journal of the Geological Society of Japan,* 124 (4), p.231-250. DOI: 10.5575/geosoc.2017.0071.

Oikawa, T., Mitsuhiro, Y., Setsuya, N., Fukashi, M., Jiro, K., Taketo, S., Yoshihiro, T., Yoshihiro, I., and Yasuhiro, I., 2016. Reconstruction of the 2014 eruption sequence of Ontake Volcano from recorded images and interviews. *Earth, Planets, and Space*, 68 (article 79), p.1-13. DOI: 10.1186/s40623-016-0458-5.

Pardo, N., Cronin, S. J., Németh, K., Brenna, M., Schipper, C. I., Breard, E., Whitte, J.D.L., Procter, J., Stewart, B., Augustin-Flores, J., Moebis, A., Zernack, A., Kereszturi, G., Lube, G., Auer, A., Neall, V., and Wallace, C., 2014. Perils in distinguishing phreatic from phreatomagmatic ash: insights into the eruption mechanisms of the 6 August 2012 Mount Tongariro eruption, New Zealand; *Journal of Volcanology and Geothermal Research,* 286, p.397-414. DOI: 10.1016/j.jvolgeores.2014.05.001.

Reimer, P.J., Bard, E., Bayliss, A., Beck, J.W., Blackwell, P.G., Bronk Ramsey, C., Buck, C.E., Cheng, H., Edwards, R.L., Friedrich, M., Grootes, P.M., Guilderson, T.P., Haflidason, H, Hajdas, I., Hatté, C., Heaton, T.J., Hoffmann, D.L., Hogg, A.G., Hughen, K.A., Kaiser, K.F., Kromer, B., Manning, S.W., Niu, M., Reimer, R.W., Richards, D.A., Scott, E.M., Southon, J.R., Staff, R.A., Turney, C.S.M., and van der Plicht, J., 2013. 'IntCal13 and Marine13

Radiocarbon Age Calibration Curves 0-50,000 Years Cal BP'. *Radiocarbon*, 55 (4), p.1869-1887. DOI: 10.2458/azu_js_rc.55.16947

Sanno, Y., Kagoshima, N., Takahata, Y., Hishio, E., Roulleau, D. L., Pinti, T., and Fischer, P., 2015. Ten-year helium anomaly prior to the 2014 Mt Ontake eruption. *Scientific Report.* DOI: 10.1038/srep13069.

Silitonga, P.H., 1973. *Geologic map of the Bandung Quadrangle, Java, scale 1:100.000*. Geology Survey Indonesia, Ministry of Mines.

Soetoyo and Hadisantono, R.D., 1992. *Geological map of Tangkuban Parahu Volcano/Sunda Complex Volcano, West Java.* Centre of Volcanological and Geology Hazard (CVGHM), Indonesia.

Sunardi, E. and Kimura, J., 1998. Temporal chemical variation in late cenozoic volcanic rocks around Bandung Basin, West Java, Indonesia. *Journal Mineralogy, Petrology, Economic Geology*, 93, p.103-128.

Suryo, I., 1981. Report of the volcanic activity in Indonesia for the period 1961-1963. *Bulletin of Volcanological Survey Indonesia, Bandung,* 104,116pp.

Suryo, I., 1985. Report of the volcanic activity in Indonesia for the period 1964-1970. *Bulletin of Volcanological Survey Indonesia, Bandung,* 106,150pp.

Suzuki, Y., Nagai, M., Maeno, F., Yasuda, A., Hokanishi, N., Shimano, T., Ichihara, M.,

Kaneko, T., and Nakada, S., 2013. Precursory activity and evolution of the 2011 eruption of Shinmoe-dake in Kirishima volcano-insights from ash samples. *Earth, Planets, and Space,* 65, p.591-607. *DOI: 10.5047/eps.2013.02.004.*

Syahidan, A., Suryantini, A., Susanto, A., and Nurdiana, A., 2015. Hydrothermal alteration study of Tangkuban Parahu Craters, and its implication to geothermal conceptual model. *Proceedings of Indonesia International Geothermal Convention and Exbition, Jakarta.*

Tregoning, P., Brunner, F.K., Bock, Y., Puntodewo, S.S., McCaffrey, R., and Genrich, J.F., 1994. First geodetic measurement of convergence across the Java Trench. *Geophysical Research Letters*, 21 (19), p.2135-2138. DOI: 10.1029/94GL01856.

Van Bemmelen, R.W., 1949. The Geology of Indonesia, Vol. 1 A. *Government. Printing Office, The Hauge.*

White, N.C. and Hedenquist, J.W., 1995. Epithermal gold deposits: styles, characteristics, and exploration. *SEG (Society of Economic Geologist) Newsletter,* 23, p.1, 9-13.

Wohletz, K. and Heiken, G., 1992. Volcanology and Geothermal Energy. *Berkeley: University of California Press*, 432pp.